JMEPEG (2012) 21:1167–1181
DOI: 10.1007/s11665-011-0062-6

1059-9495/$19.00

An Experimental Evaluation of Material Properties and Fracture Simulation of Cryorolled 7075 Al Alloy

Prosenjit Das, I.V. Singh, and R. Jayaganthan

(Submitted May 29, 2011; in revised form August 26, 2011)

This work presents an experimental evaluation of yield strength, tensile strength, and impact toughness of 7075 Al alloy. The extended finite element method (XFEM) has been chosen for quasi-static crack growth simulations using Charpy impact energy as the crack growth criterion for both Bulk and ultrafine-grained (UFG) 7075 Al alloy. The 7075 Al alloy is rolled for different thickness reductions (40 and 70%) at cryogenic (liquid nitrogen) temperature, and its mechanical properties are studied by performing the tensile and Charpy impact testing. The microstructural characterization of the alloy was carried out using field emission scanning electron microscopy (FE-SEM). The rolling of the Al alloy at cryogenic temperature suppresses dynamic recovery, and dislocation cells formed during processing, transformed into fully formed ultrafine-grains (600 nm) at 70% thickness reduction. The impact energy used as the crack growth criterion under quasi-static loading condition based on the Griffith energy concept. The elastic-plastic ductile fracture simulations are performed by XFEM using ABAQUS Software (Version 6.9). For crack modeling, two different types of functions are used to model a crack based on partition of unity concept. A discontinuous function is used to model the portion behind the crack tip, whereas crack tip is modeled by near-tip asymptotic functions. This permits the crack is to be represented explicitly without meshing the crack surfaces, thus crack propagation simulations can be carried out without a need of re-meshing. Strain energy release and stress distribution ahead of the crack tip is found for some practical crack problems. The numerical examples indicate a significant improvement in crack growth properties of UFG 7075 Al alloy as compared to its bulk form due to an effective grain refinement.

Keywords cryorolling, elastic-plastic fracture, impact toughness, UFG alloy, XFEM, yield strength

1. Introduction

In recent years, the production of ultrafine-grained (UFG) and nanostructured materials from their bulk materials through severe plastic deformation (SPD) processes like equal channel angular pressing (ECAP), multiple compressions, and severe torsional straining have been given lot of focus to realize its potential for structural and functional applications. The formation of ultrafine grain structures by SPD methods provides very large deformations at relatively low temperatures under high pressures (Ref 1, 2). In this work, ultrafine-grained 7075 Al alloy is prepared by doing conventional rolling at cryogenic (liquid nitrogen) temperature (Ref 3, 4). Rolling at cryogenic temperature suppresses dynamic recovery, and the density of accumulated dislocations reaches to a higher steady state level as compared to room temperature rolling. With the multiple cryorolling passes, these high density dislocations are converted into grain fragments or ultrafine grain structures with high angle grain boundaries. Ultrafine-grained form of Cu, Ni, Al alloys shows improved tensile and hardness properties as reported in the earlier literature (Ref 3-6).

The 7075 aluminum alloy is one of the most important engineering alloys and has been utilized extensively in aircraft structures because of its high strength-to-density ratio (Ref 3, 4, 7). In the present work, tensile and impact properties of the bulk 7075 Al alloy as well as its UFG form are experimentally evaluated. Experimental results show a significant improvement in the tensile and impact toughness.

There is no published literature which describes the fracture behavior of UFG 7075 Al alloy using extended finite element method (XFEM). Therefore, in the present work, the fracture behavior of UFG 7075 Al alloy compared to its bulk form has been studied. The fracture energy absorbed by Charpy impact specimens of both bulk and UFG alloys are used as the crack growth criterion for XFEM simulations. The XFEM crack growth simulations are carried out under quasi-static loading (Ref 8-10). An explicit crack propagation criterion for elastic-plastic ductile fracture is derived based on the Griffith energy concept. The capability of XFEM to accurately simulate the fracture behavior is proved through several numerical examples. In case of ductile fracture, nonlinearities arise due to plastic deformation of the bulk material and the crack surface separation in the fracture process zone, which are characterized by the nucleation, growth and coalescence of micro-voids (Ref 11-13). Mesh independent crack propagation simulations are carried out using XFEM in the elastic-plastic regime (Ref 14-18) under quasi-static Mode-I loading following the deformation plasticity theory (Ref 12). A brief description of

Prosenjit Das, Foundry Section, Central Mechanical Engineering Research Institute, Durgapur 713209, India; **I.V. Singh**, Department of Mechanical and Industrial Engineering, Indian Institute of Technology Roorkee, Roorkee 247667, India; and **R. Jayaganthan**, Department of Metallurgical and Materials Engineering & Centre of Nanotechnology, Indian Institute of Technology Roorkee, Roorkee 247667, India. Contact e-mail: ivsingh@gmail.com.

XFEM and energy criterion for the crack growth is given in "Extended Finite Element Method" and "The Energy Criterion for Crack Growth" sections, respectively.

2. Extended Finite Element Method

In comparison to the classical finite element method, the XFEM provides significant benefits in the numerical modeling of crack propagation. In the traditional formulation of the FEM, the existence of a crack is modeled in such a way that the crack need to follow element edges, whereas in the XFEM, the crack geometry need not be aligned with the element edges, which provides flexibility and versatility in crack modeling (Ref 19, 20). The XFEM is based on the enrichment of the FE model with additional degrees of freedom (DOFs) that are tied to the nodes of the elements intersected by the crack. XFEM utilizes the concept of partition of unity (PU) for the enrichment. Any discontinuity is included in the numerical model without modifying a mesh as it is initially generated without taking into account the presence of the crack. Therefore, only a single mesh is required for the modeling of any size of crack. In addition, nodes surrounding the crack tip are enriched with DOFs associated with functions that reproduce the asymptotic fracture fields.

In XFEM, the following approximation is utilized to calculate the displacement for a point **x** within the domain (Ref 21).

$$u^h(x) = u^{\mathrm{FE}} + u^{\mathrm{enr}} = \sum_{j=1}^{n} N_j(x)u_j + \sum_{k=1}^{m} N_k(x)\,\psi(x)a_k \qquad \text{(Eq 1)}$$

where u_j is the vector of regular degrees of nodal freedom in the finite element method, a_k is the added set of degrees of freedom to the standard finite element model, and $\psi(x)$ is the discontinuous enrichment function defined for enriched nodes. The main objectives for using various types of enrichment functions within an XFEM procedure can be expressed as the following:

- Reproducing the singular field around a crack tip.
- Continuity in displacement between adjacent finite elements.
- Independent strain fields in two different sides of a crack surface.

In general, two types of enrichment functions are used, i.e., Heaviside function, H(x) and crack-tip functions. If there is no enrichment, then the above Equation 1 reduces to the classical finite element approximation $u^h(x) = \sum_{j=1}^{n} N_j(x)u_j$, hence, XFEM retains many of the advantages of the finite element method. Figure 1 shows the types of enrichment functions used in XFEM crack modeling.

3. The Energy Criterion for Crack Growth

The fracture energy obtained by Charpy Impact testing is used as the crack growth criterion under quasi-static loading based on the Griffith energy concept. The equations given here are limited to quasi-static crack growth only. The functional relationship of Charpy impact energy is:

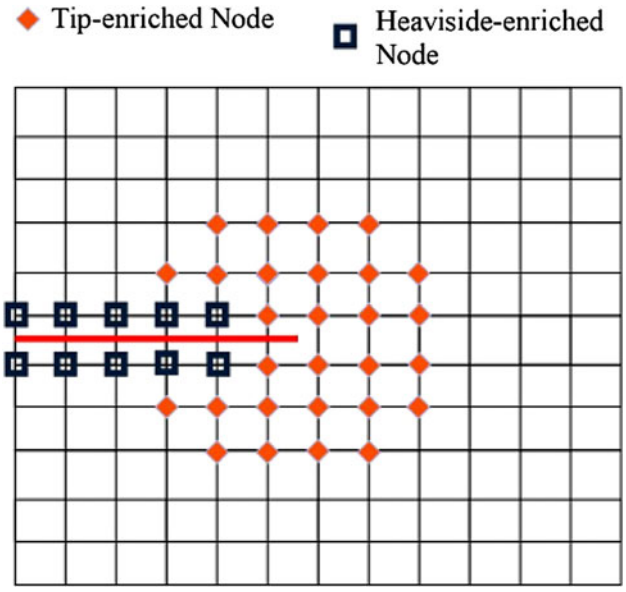

Fig. 1 Enriched nodes in the XFEM: square nodes with two additional DOFs and diamond-shaped nodes with eight additional DOFs (Ref 10)

$$E_{\mathrm{T}} = E_{\mathrm{I}} + E_{\mathrm{P}} \qquad \text{(Eq 2)}$$

where E_{T} = total fracture energy, E_{I} = fracture initiation energy, and E_{P} is fracture propagation energy. The fundamental principle of energy conservation with respect to unit area crack extension (Ref 22) is same as Griffith fracture mechanics criterion (Griffith, 1921) which can be mathematically stated as (Ref 11):

$$T_{\mathrm{r}} = \frac{\partial}{\partial A}(W_{\mathrm{F}} - U_{\mathrm{e}} - U_{\mathrm{P}} - E_{\mathrm{s}}) \text{ with } \begin{cases} T_{\mathrm{r}} > E_{\mathrm{T}} & \text{Crack propagates} \\ T_{\mathrm{r}} = E_{\mathrm{T}} & \text{Critical condition} \\ T_{\mathrm{r}} < E_{\mathrm{T}} & \text{Crack does not propagate} \end{cases} \qquad \text{(Eq 3)}$$

where T_{r} is the resultant energy, U_{e} is the elastic strain energy, and U_{p} is the plastic strain energy, respectively. W_{F} is the work done by the externally applied loadings, E_{s} is the surface energy, and A is the total crack surface area (Ref 23-25). The result of first two terms in Equation 3 is the strain energy release rate (G) which is considered as a driving force for crack growth:

$$G = \frac{\partial(W_{\mathrm{F}} - U_{\mathrm{e}})}{\partial A} \qquad \text{(Eq 4)}$$

The last two terms of Equation 3 represent the plastic energy dissipation rate and the energy dissipation rate due to crack surface separation. The summation of these two terms represents the crack growth resistance, which is defined as "energy dissipation rate" R.

$$R = \frac{\partial(U_{\mathrm{p}} + E_{\mathrm{S}})}{\partial A} \qquad \text{(Eq 5)}$$

Equation 3 says that whenever the crack driving force exceeds the crack resistance force, the crack will propagate. In context of FEM, the external work P and the total strain energy of the system U can be expressed, respectively, as,

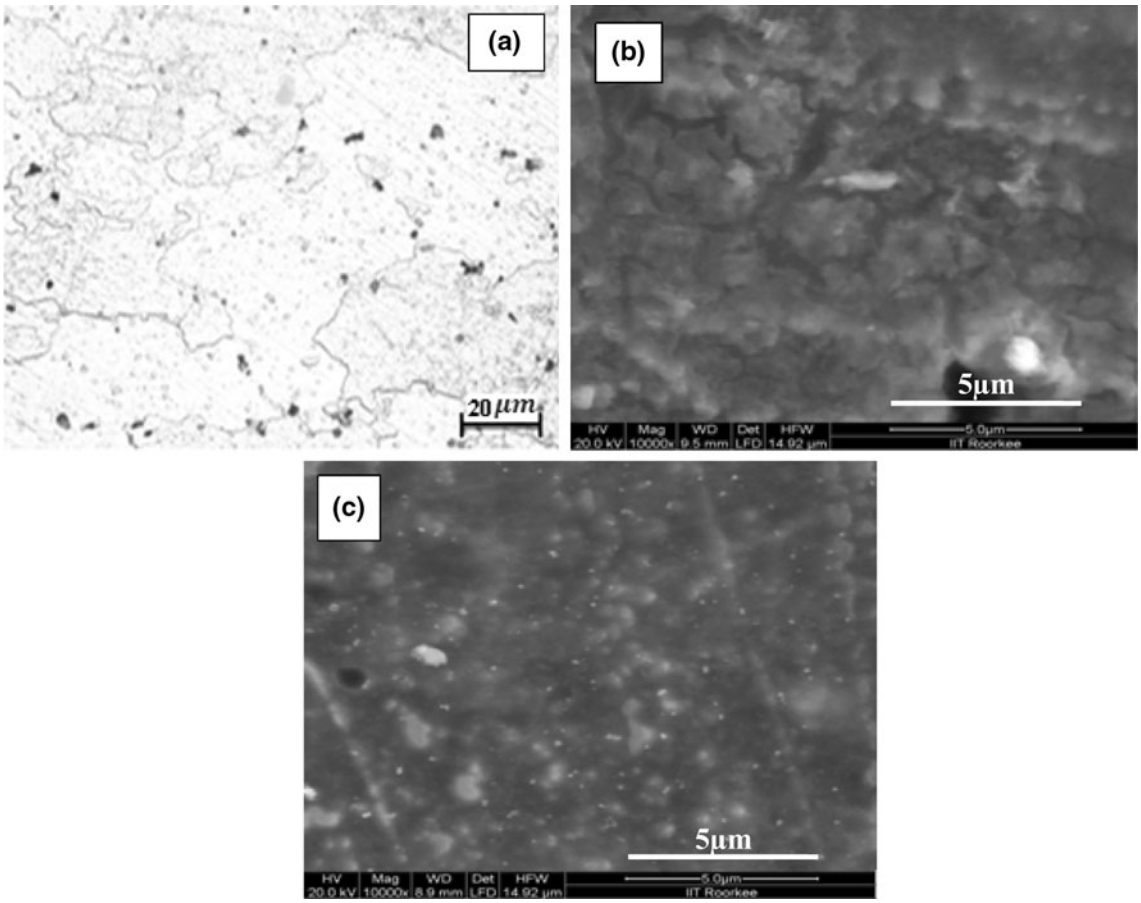

Fig. 2 (a) Optical micrograph of starting material and FESEM image of (b) 40 CR and (c) 70 CR

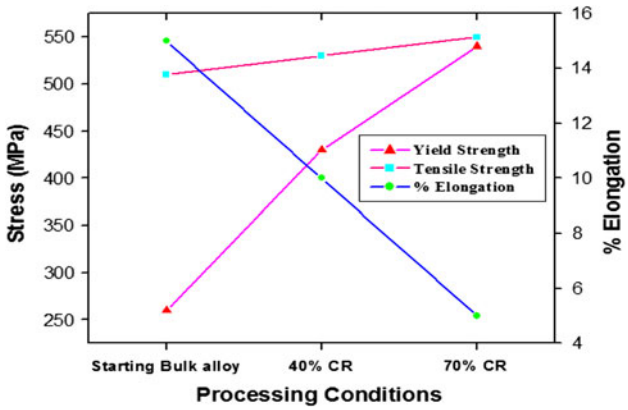

Fig. 3 Tensile properties of Al 7075 alloy after different percentage of thickness reduction

$$P = \mathbf{u}^{\mathrm{T}}\mathbf{F} \quad \text{(Eq 6)}$$

$$U = U_{\mathrm{e}} + U_{\mathrm{p}} = \int_{V} W dV \quad \text{(Eq 7)}$$

where V is the volume, $\mathbf{u}$ the nodal displacement vector, $\mathbf{F}$ the nodal equivalent force vector, respectively, and W the total strain energy density. The volume integration in Equation 7 can be carried out on element by element basis. The strain energy of each element is calculated for all the elements.

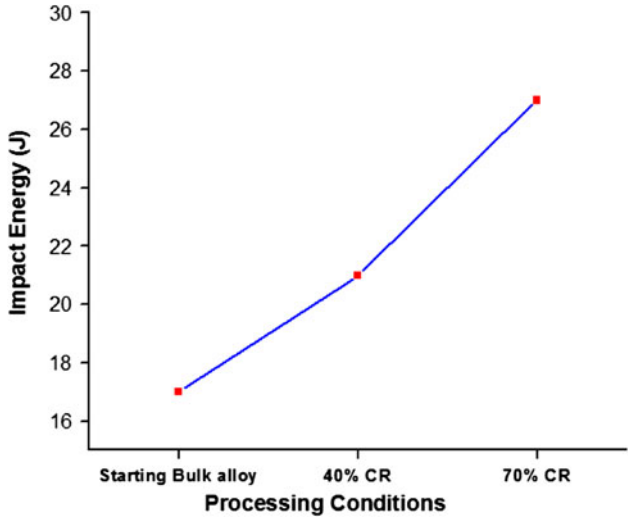

Fig. 4 Effect of cryorolling on the impact energy of 7075 Al alloy

4. Experimental Procedure

The 7075 Al alloy has been procured from Hindustan Aeronautics Ltd., Bangalore, India in the form of extruded ingot having 50 mm diameter, for the present work. Chemical composition of the alloy used in the work was estimated using Energy Dispersive Spectroscopy (EDAX) investigation. The

Table 1 Elastic-plastic material properties of the 7075 Al alloy under investigation

Material	*E*, GPa	υ	σ_y, MPa	*n*
Al 7075 alloy (Bulk)	72	0.33	260	10
Al 7075 alloy (UFG-70% CR)	72	0.33	540	12

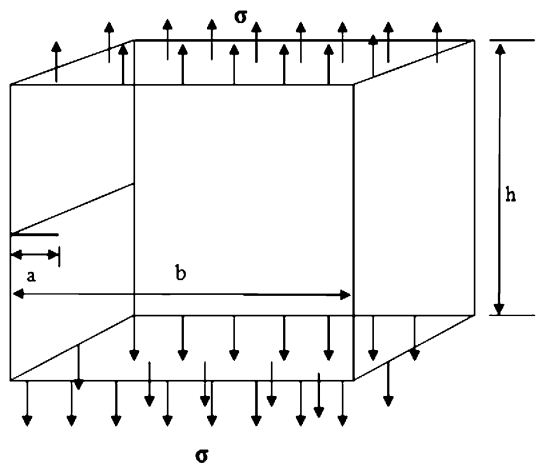

Fig. 5 Edge crack under uniaxial tension in 3D

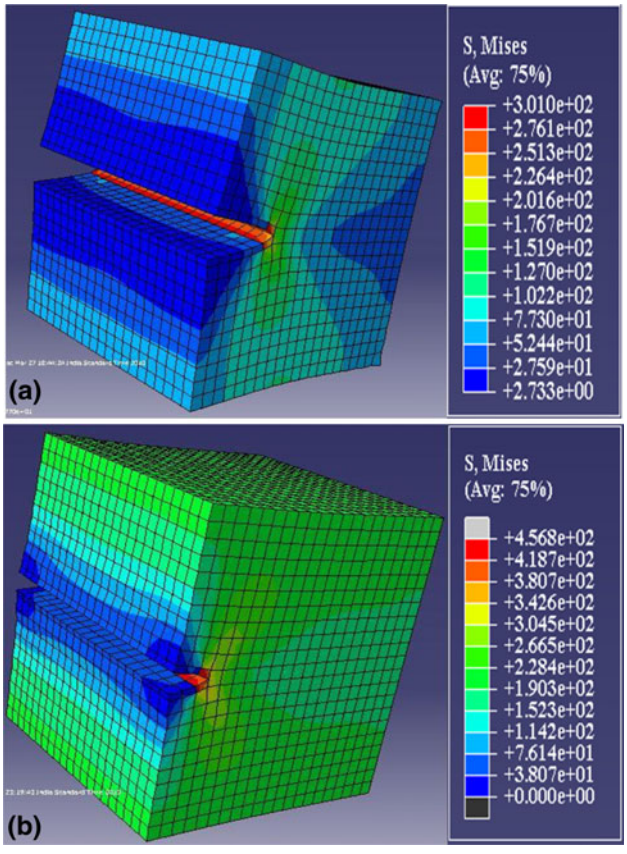

Fig. 6 A comparison of Von Mises stress distribution around crack tip. (a) Bulk and (b) UFG 7075 Al alloy

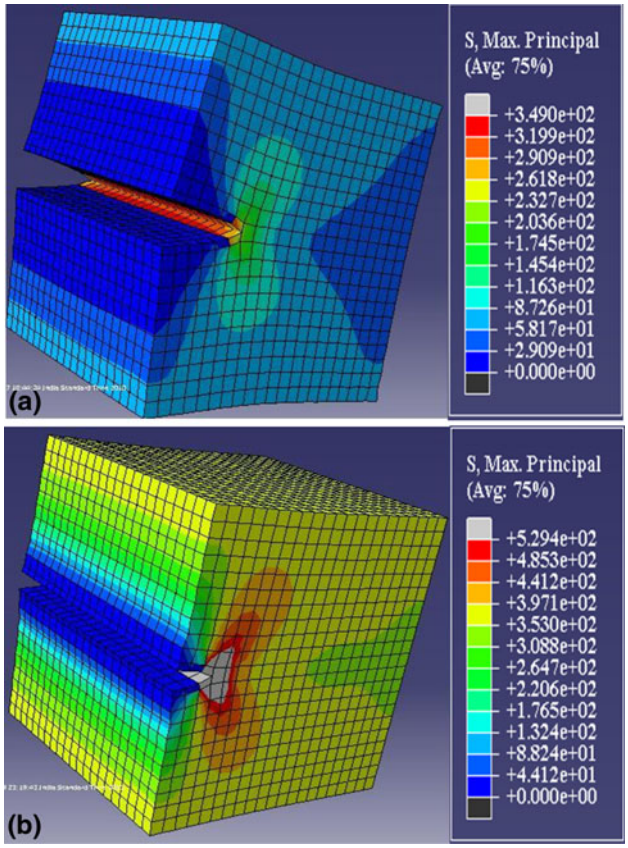

Fig. 7 A comparison of maximum principal stress distribution around crack tip. (a) Bulk and (b) UFG 7075 Al alloy

composition was 6.04 Zn, 3.64 Mg, 1.76 Cu, 0.50 Cr, 0.2 Si, 0.15 Mn, 0.57 Fe, and Al balance. The as-received Al ingot was machined into small plates and then solution treated (ST) at 490 °C for 6 h followed by quenching treatment in water at room temperature. The annealed plates of 7075 Al alloy were subjected to rolling at liquid nitrogen atmosphere (cryorolling) to achieve 40 and 70% thickness reduction. The samples were dipped in liquid nitrogen for 30 min prior to each roll pass during the rolling process. The diameter of the rolls was 110 mm and the rolling speed was 8 rpm. −190 and −150 °C were the temperatures before and after rolling of the samples in each pass. The solid lubricant, $MoSi_2$, has been used during the rolling process to minimize the frictional heat and 40-50 s time taken for rolling and putting back the samples into cryocan (liquid nitrogen container) in order to preclude the temperature rise of the samples. Though 5% deformation (in comparison of the starting thickness) achieved per rolling pass, still many passes were given to achieve the required reduction of the samples, to ensure ultrafine-grain formation throughout the cross-section of the samples.

In order to evaluate the strength and ductility, tensile tests were carried out of the starting Al-Mg-Cu-Zn alloy and its cryorolled forms. The tensile specimens were machined as per ASTM Standard E-8/E8M-09 (Ref 26) sub-size specifications parallel to the rolling direction with gauge lengths of 25 mm. The tensile test was conducted after polishing the samples in air at room temperature using a S series, H25K-S materials testing machine operated at a constant crosshead speed with an initial strain rate of 5×10^{-4} s^{-1}. For tensile test, the samples with

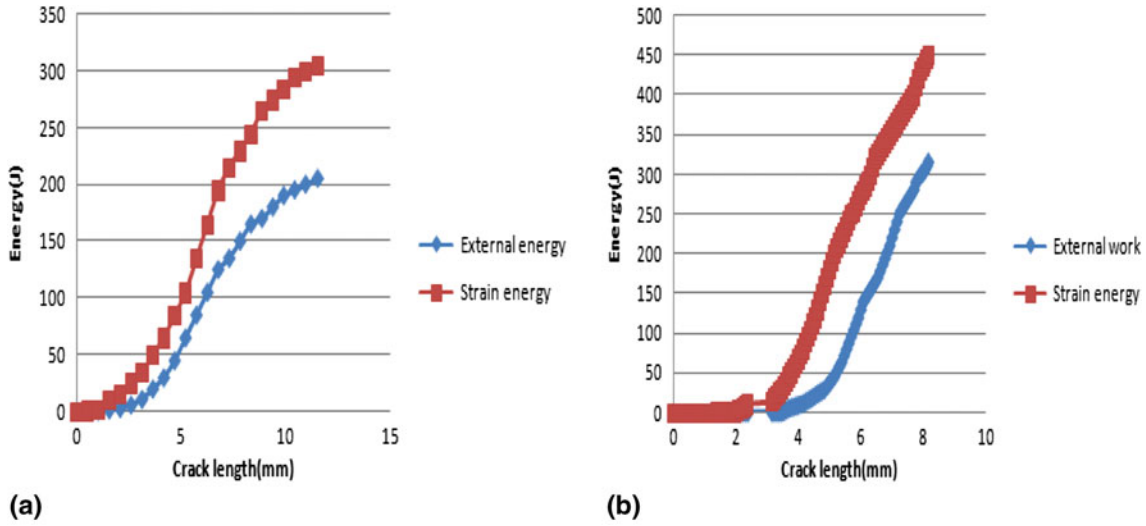

Fig. 8 A comparative plot of strain energy release for (a) bulk and (b) UFG 7075 Al alloy

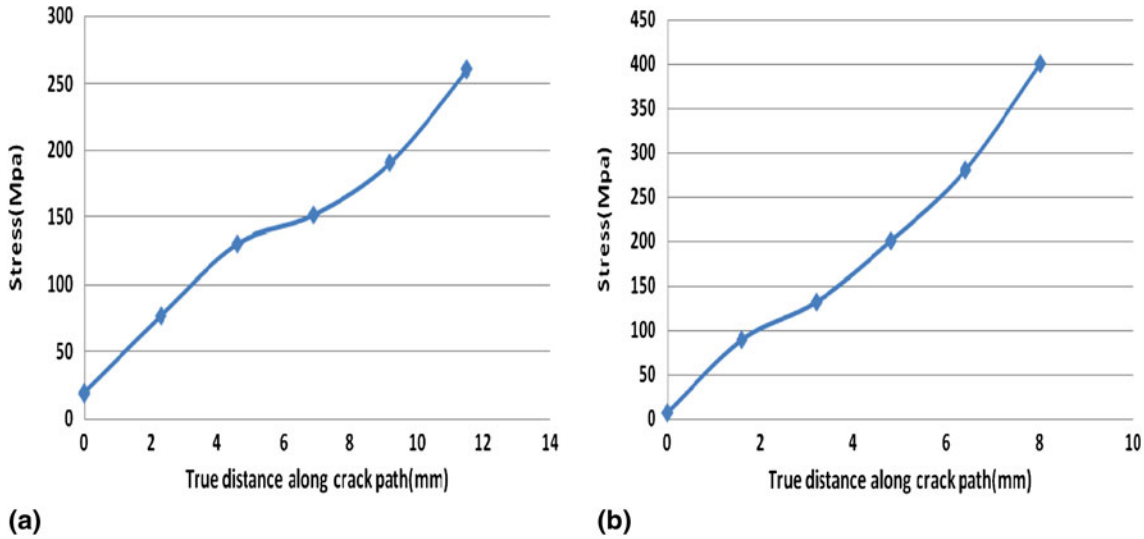

Fig. 9 A comparison of stress for (a) bulk and (b) UFG 7075 Al alloy

different percentage of thickness reduction after cryorolling were machined to the same length and without changing the thickness.

For the evaluation of fracture energy, impact test is carried out using Charpy impact specimens. Test samples were cut from longitudinal (rolling) direction. The in-plane specimen dimensions as per the ASTM Standard E-23-07ae1 (Ref 27) was, 10 mm × 55 mm rectangular block with a 2 mm deep, 45° V-notch having a 0.25-mm tip radius at the center of the specimen. In this paper, the results are presented from CVN impact tests on staring bulk and UFG form of the said alloy.

5. Results and Discussion

5.1 Experimental Results

Figure 2 reveals microstructural features of the bulk and UFG 7075 Al alloy. The optical micrograph of the starting bulk alloy shown in Fig. 2(a) and SEM micrographs of the cryorolled alloys are shown in Fig. 2(b) and (c). Lamellar grains (average grain size is around 40 μm) lying parallel to the ingot axis were observed in case of bulk alloy, whereas equiaxed (in the rolling direction) grains were seen in case of UFG alloys. The grain size is reduced to around 950 and 600 nm for the CR samples subjected to 40 and 70% thickness reduction, respectively. Due to rolling at cryogenic temperature (−190 °C), grain growth, dynamic recovery is effectively suppressed and grain fragmentation, sub grain formation, ultrafine grains with high angle grain boundaries are formed as reported in our earlier work (Ref 28-31).

Tensile properties of bulk and UFG 7075 Al alloy is estimated by testing a set of five samples for each condition and average values are shown in Fig. 3. Increase in tensile strength (UTS) for 40% (true strain = 1.4) and 70% reduction (true strain = 1.8) are 530 MPa (nearly 6% increase) and 550 MPa (nearly 10% increase), respectively, from 500 MPa of bulk

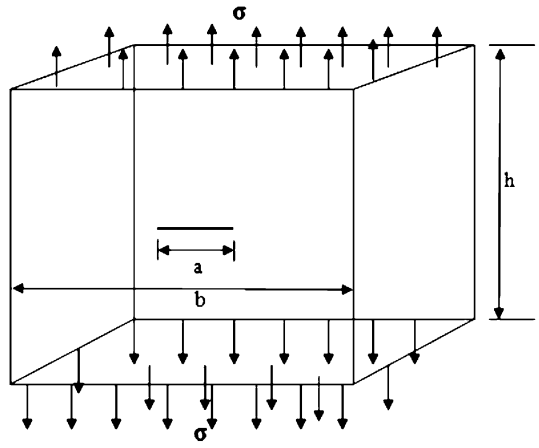

Fig. 10 Center crack under uniaxial tension in 3D

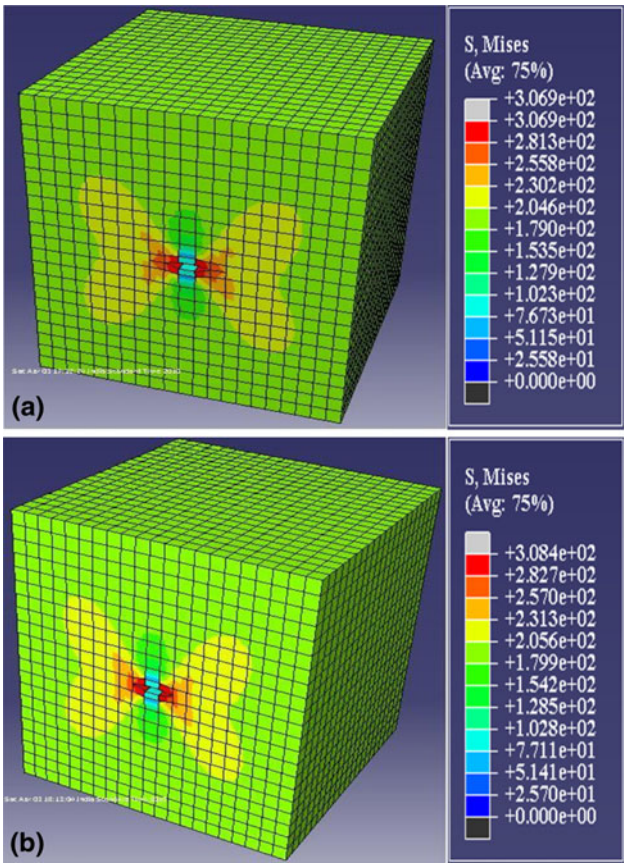

Fig. 11 A comparison of Von Mises stress distribution around crack tip. (a) Bulk and (b) UFG 7075 Al alloy

material. The yield strength (YS) has increased to 430 MPa (nearly 66% increase) and 540 MPa (nearly 108% increase) for 40 and 70% reduction from 260 MPa of bulk alloy. Rolling at cryogenic temperature can effectively suppress the dynamic recovery, grain growth and generates higher amount of dislocation cells and fragmented grains in the samples which leads to enhanced tensile strength of the Al-Mg-Zn-Cu alloy (Ref 29, 31). More pronounced effect in YS as compared to the

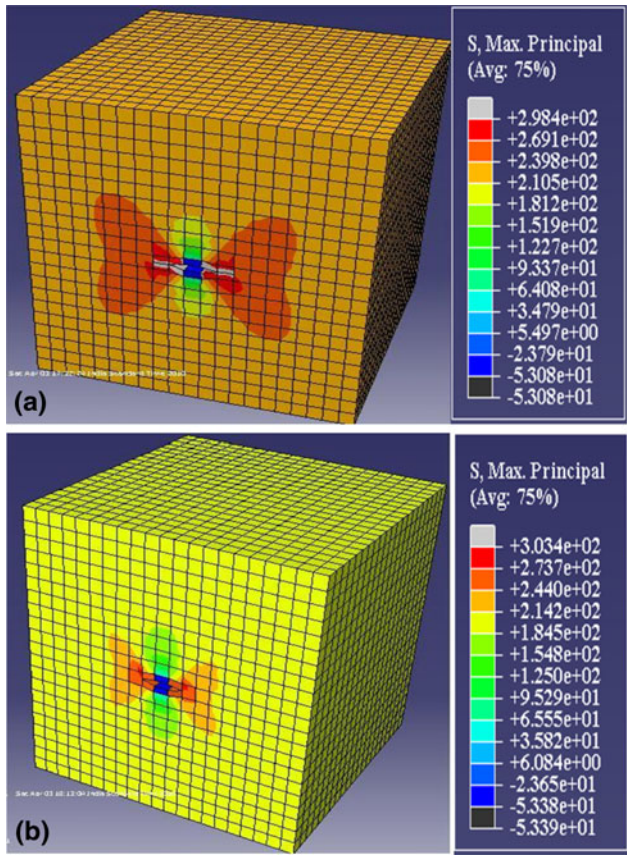

Fig. 12 A comparison of maximum principal stress distribution around crack tip. (a) Bulk and (b) UFG 7075 Al alloy

ultimate tensile strength (UTS) of the cryorolled alloy is due to effective grain refinement, which can be explained from simple Hall-patch relationship.

Impact energy absorbed in the UFG samples of 7075 Al alloy and its bulk counterpart are estimated by testing a set of five samples for both bulk and UFG alloy and average values are shown in Fig. 4. The impact energy of the cryorolled alloy increases due to the breakage of large aluminum dendrites, modified grain or grain fragment with high angle boundaries, sub-grain formation, and ultrafine grain or grain fragments with the enhanced amount of cryorolling strain. Impact energy of the bulk alloy and its UFG counterpart are 17 J, 21 J (24% increase) in case of 40% reduction and 27 J (nearly 60% increase) in case of 70% reduction.

5.2 Fracture Surface Morphology

Tensile and impact fracture morphologies were discussed in detail as reported in our earlier work (Ref 29).

5.2.1 Tensile Fracture. Fractographs of tensile samples of starting bulk Al 7075 alloy and UFG alloys (40 and 70% cryorolled) reveals that fracture mode is of ductile nature for both the bulk and UFG Al alloy specimens. The average dimple size is reduced to less than 1 μm after 70% thickness reduction in the cryorolled samples from 5 μm of the starting bulk alloy. Grain refinement and work hardening are the possible mechanisms responsible for the continuous decrease in dimple size, attained by cryorolling process.

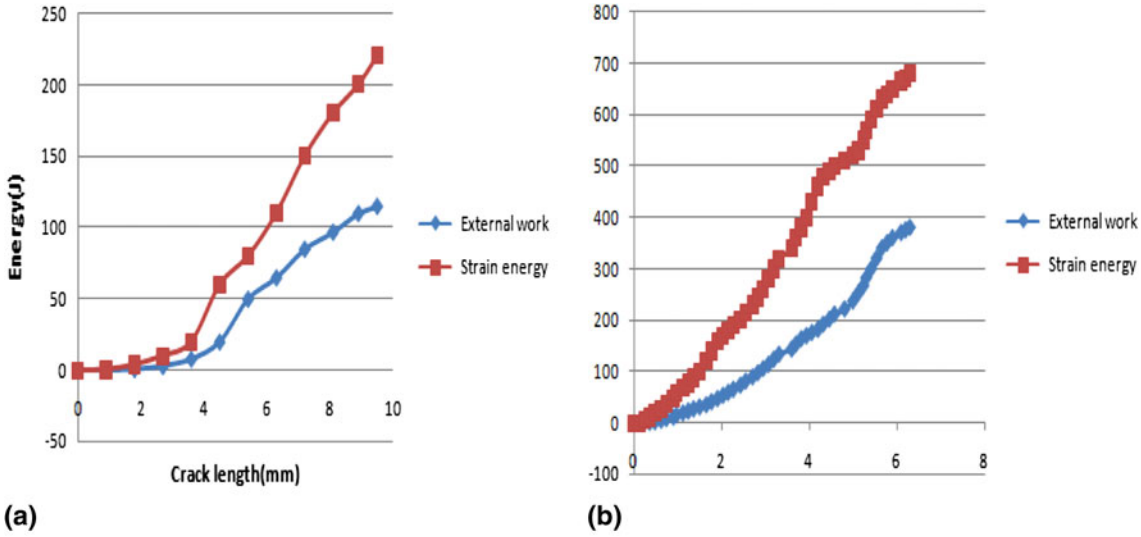

Fig. 13 A comparative plot of strain energy release for (a) bulk and (b) UFG 7075 Al alloy

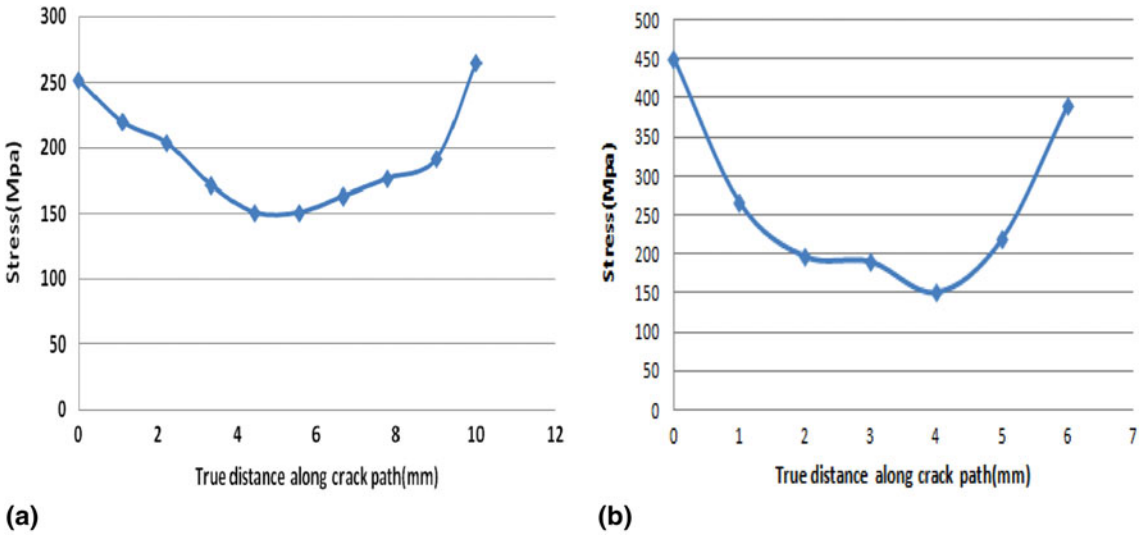

Fig. 14 A comparison of stress for (a) bulk and (b) UFG 7075 Al alloy

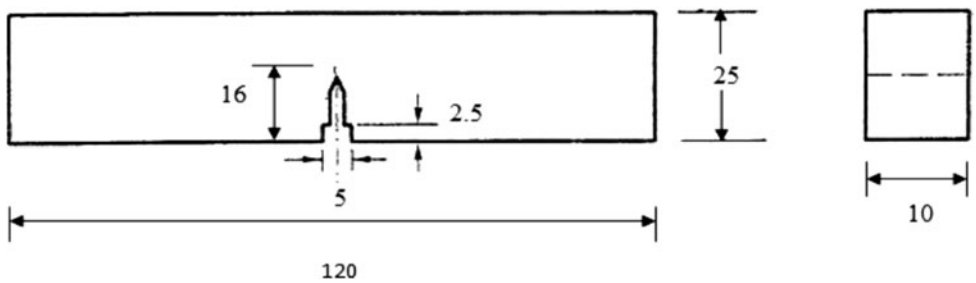

Fig. 15 Schematic diagram of three-point bend specimen (all dimensions are in mm)

5.2.2 Impact Fracture. The fracture behavior of the samples tested under impact load is different from that of tensile test due to high strain rate involved in case of impact loading. The fracture surface shows complete dimple fracture as compared to some quasi-cleavage regions present in the case of tensile fracture surface. The continuous decrease in dimple size with the increase in % reduction obtained by cryorolling, make the evidence of enhanced fracture energy in case of UFG alloys.

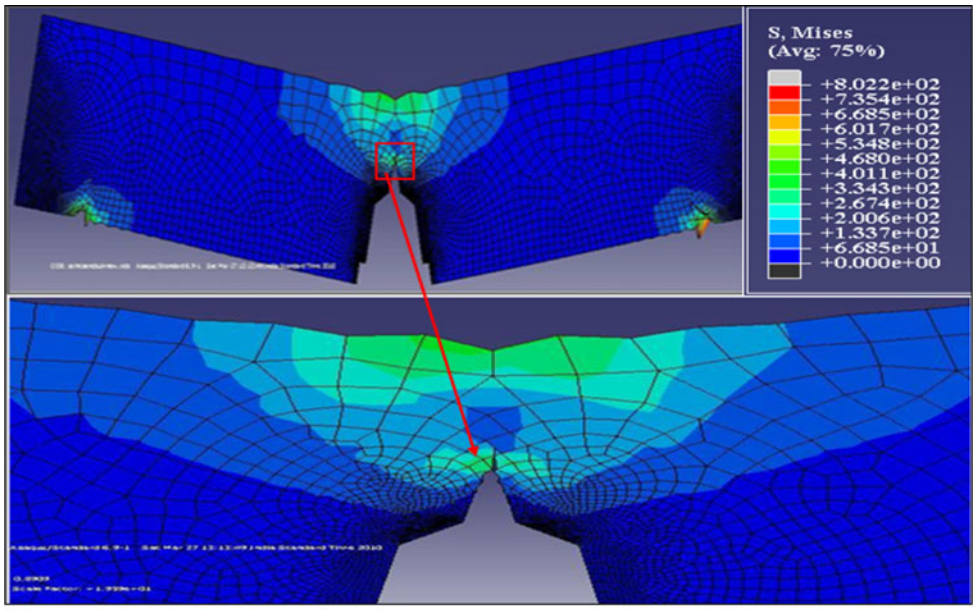

(a)

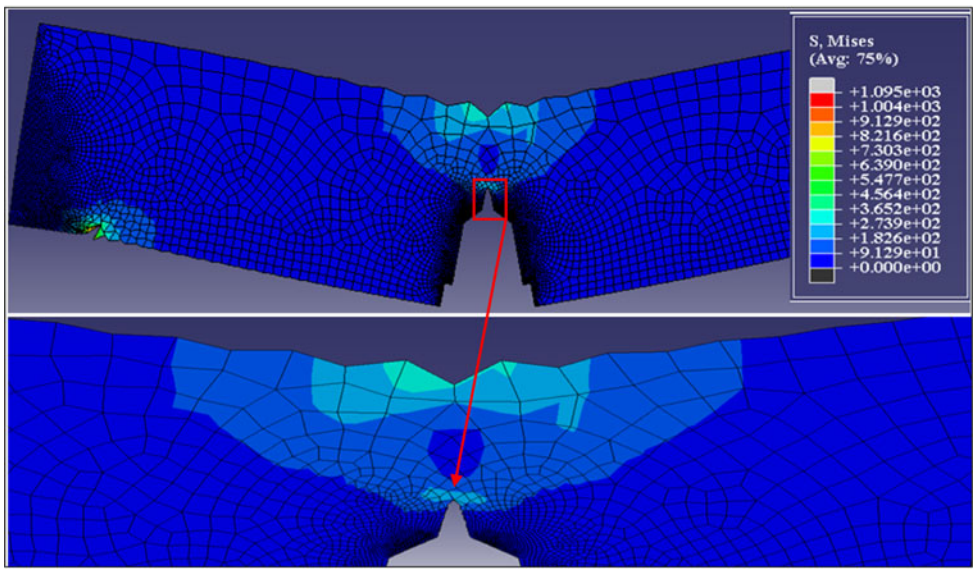

(b)

Fig. 16 A comparison of Von Mises stress distribution around crack tip. (a) Bulk 7075 Al alloy (zoomed view at the crack tip), (b) UFG 7075 Al alloy (zoomed view at the crack tip)

5.3 XFEM Simulation

Elastic-plastic material properties of both UFG and bulk 7075 Al alloy, evaluated experimentally were used for XFEM simulation of predicting the fracture behavior using standard finite element software ABAQUS, based on deformation plasticity theory. To demonstrate the improved fracture properties of UFG 7075 Al alloy as compared to its bulk counterpart, the strain energy release rate, stress distribution ahead of the crack tip (Ref 11), crack propagation study, and plastic zone size ahead of the crack tip are evaluated for several test problems.

Table 1 shows the improved elastic-plastic material properties of the cryorolled 7075 Al alloy along with its bulk form. Mesh independent crack propagation simulations has been carried out under quasi-static Mode-I loading using the eformation plasticity theory based on Ramberg-Osgood relationship (Ref 12, 32). In case of deformation plasticity, the material behavior is modeled by a polynomial popularly known as Ramberg-Osgood relation. It models the material behavior (elastic-plastic) by one function only. Stress and strain involving plastic deformation have the following relationship,

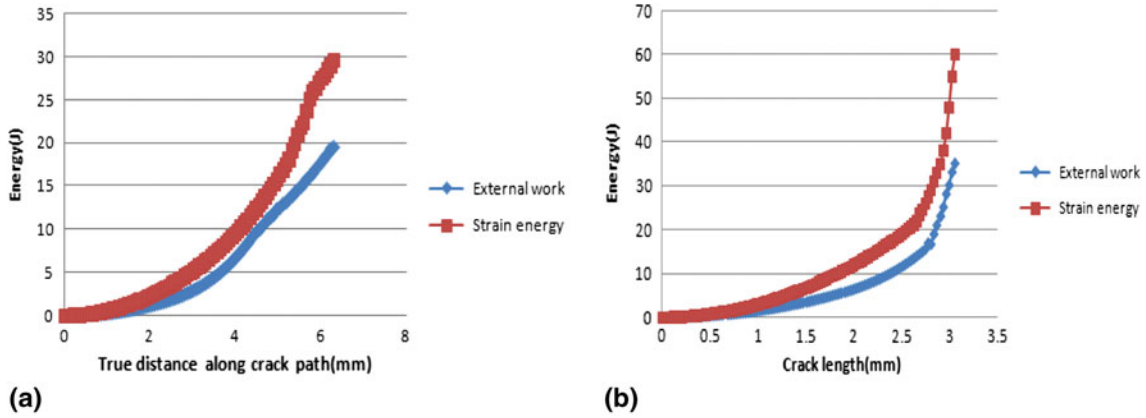

Fig. 17 A comparative plot of strain energy release for (a) bulk and (b) UFG 7075 Al alloy

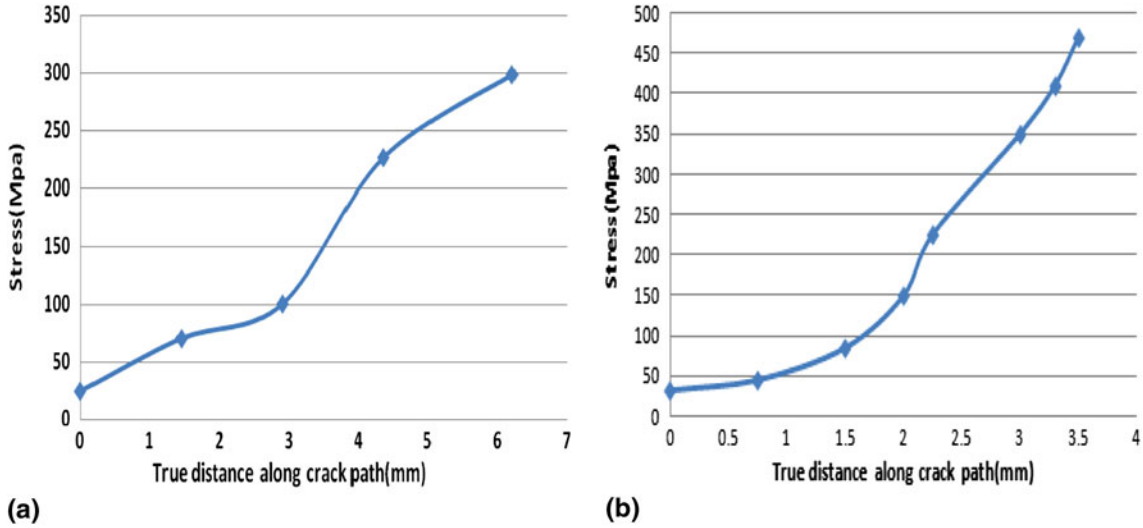

Fig. 18 A comparison of stress for (a) bulk and (b) UFG 7075 Al alloy

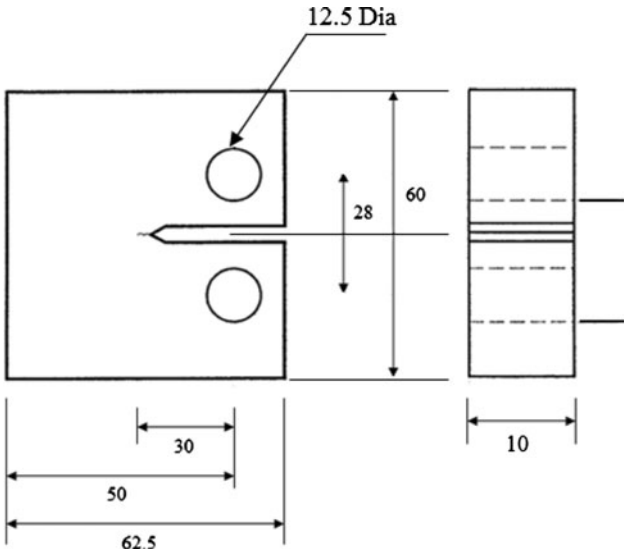

Fig. 19 Schematic diagram of compact tension specimen (all dimensions are in mm)

$$E \cdot \varepsilon = \sigma + \alpha\left(\frac{\pm\sigma}{\sigma_0}\right)^{n-1}\sigma \qquad \text{(Eq 8)}$$

where σ is the stress, ε is the strain, E is Young's modulus, α is the "yield" offset, and n (>1) is the hardening exponent (non-linear term) for the plastic deformation. In the current model, strain energy density is computed by Equation 8, as given below,

$$W = \int \sigma \, d\varepsilon \qquad \text{(Eq 9)}$$

The method followed for stress solutions in the corresponding nonlinear material model is shown below. Considering $q = \pm\sigma$, Eq. (8) solved for σ using Newton's method. Writing c_σ as the correction to σ, the Newton equations for Equation 8, are

$$\left[1 + n\alpha\left(\frac{q}{\sigma_0}\right)^{n-1}\right] c_\sigma = E\varepsilon - \sigma - \alpha\left(\frac{q}{\sigma_0}\right)^{n-1}\sigma \qquad \text{(Eq 10)}$$

$$\sigma = \sigma - c_\sigma \qquad \text{(Eq 11)}$$

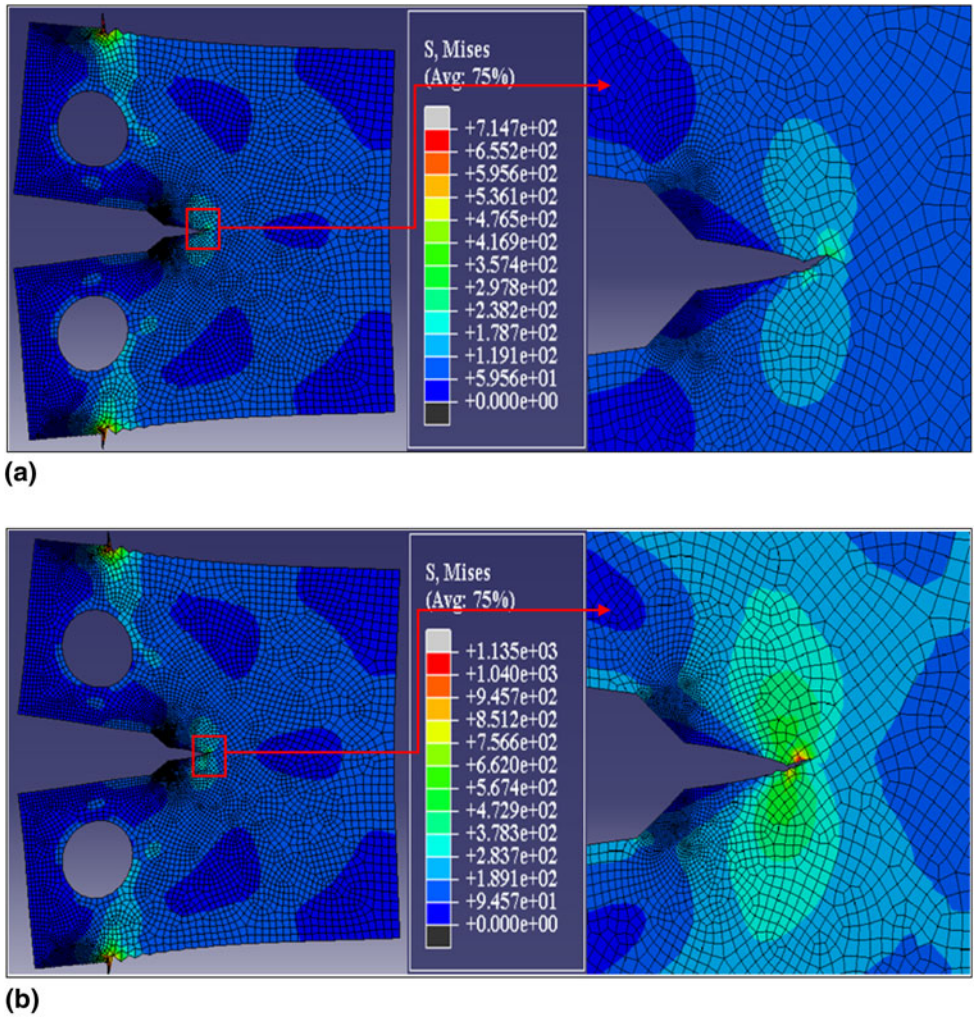

Fig. 20 A comparison of Von Mises stress distribution around crack tip. (a) Bulk 7075 Al alloy (zoomed view at the crack tip), (b) UFG 7075 Al alloy (zoomed view at the crack tip)

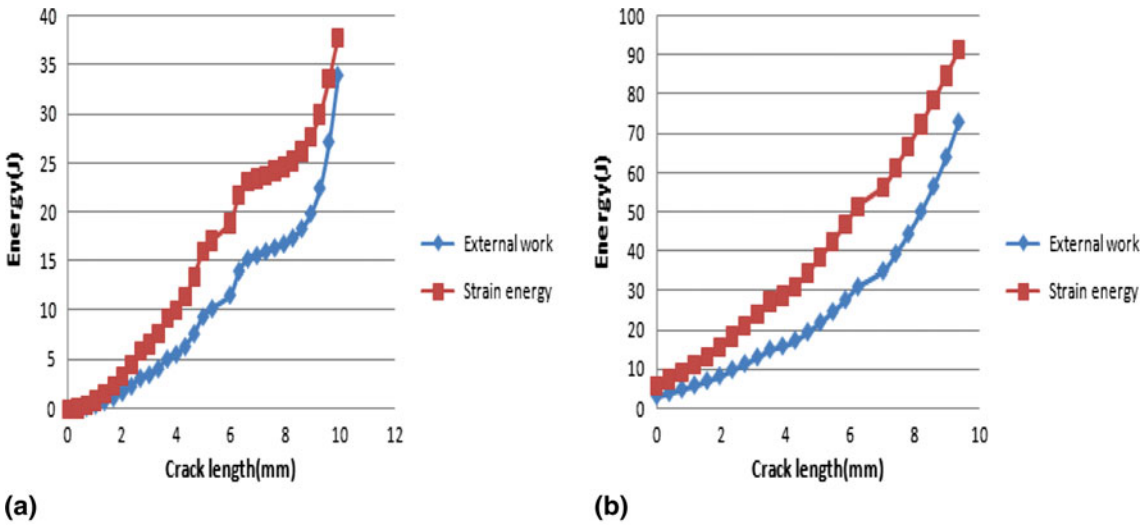

Fig. 21 A comparative plot of strain energy release for (a) bulk and (b) UFG 7075 Al alloy

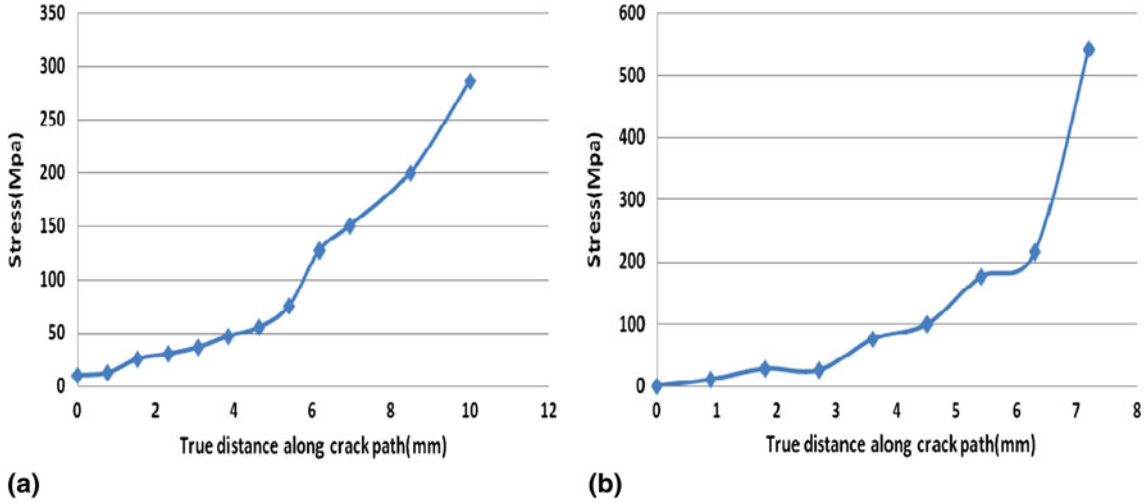

Fig. 22 A comparison of stress for (a) bulk and (b) UFG 7075 Al alloy

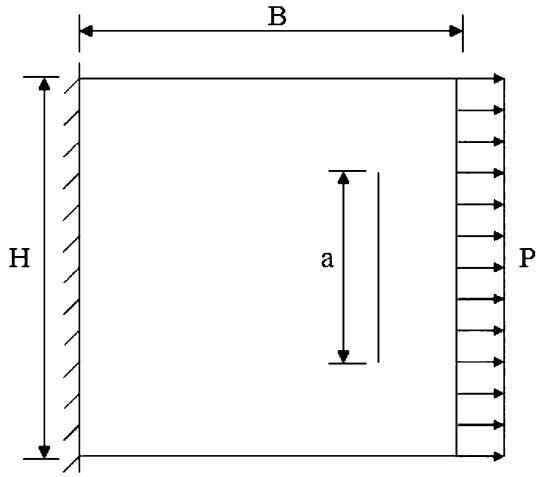

Fig. 23 Cracked plate with temperature distribution

As an initial guess, we use $\sigma = E\varepsilon$, if $E\varepsilon \leq \sigma_0$ and $\sigma = \pm[E\varepsilon\sigma_0^{n-1}/E\varepsilon\sigma_0^{n-1}\alpha\cdot\alpha]^{1/n}$, if $E\varepsilon \leq \sigma_0$. In this case, the material stiffness matrix is,

$$\frac{\partial\sigma}{\partial\varepsilon} = \frac{E}{1 + n\sigma(q/q_0)^{n-1}} \qquad \text{(Eq 12)}$$

5.3.1 Case 1: Edge Crack in Tension. Figure 5 shows the geometry of the 3D edge crack block having height (h = 40 mm), width (b = 40 mm), thickness (t = 40 mm) and a through thickness crack length on both the edges (a = 7 mm). The value of uniaxial tensile stress (σ) applied is 100 MPa. Edge crack geometry has been modeled by unstructured mesh using bilinear quadrilateral (reduced integration plain strain) elements having 41 elements along the edges. Present research reports about elastic-plastic ductile fracture of bulk 7075 Al alloy and its UFG form. The stress components with the failure mechanism for the 3D edge crack problem are shown in Fig. 6 and 7. These figures also show the bigger plastic zone size ahead of the crack tip due to ultrafine-grain formation.

Figure 8 shows that for the edge crack problem under same loading, geometric, and displacement/rotation boundary conditions. The strain energy release and external work is found more in case of ultrafine grain 7075 Al alloy as compared to bulk alloy due to higher plastic strain work involved in the fracture process zone ahead of the crack tip.

In Fig. 9, stress values plotted along the crack path shows the highest values of stresses near the crack tip for both the materials. High stress values is seen ahead of the crack tip in UFG alloy due to more stress requirement for local yielding which explains its improved crack arrest capabilities.

Experimental observation of improved crack arrest capabilities and enhanced fracture toughness in case of cryorolled samples is due to high density of dislocations, ultrafine-grain formation, grain boundary sliding, and increased fracture stress (σ_f) according to Equation 13.

$$\sigma_f = k_f d^{-1/2} \qquad \text{(Eq 13)}$$

where k_f = Constant (MPa $m^{1/2}$) and d = Grain size.

Fracture toughness of bulk Al alloy is increased from 17.89 MPa $m^{1/2}$ to 24 MPa $m^{1/2}$ (34% increase) and 30.84 MPa $m^{1/2}$ (nearly 73% increase) after 40 and 70% thickness reductions, respectively. The experimental outcomes are discussed in detail in our earlier work (Ref 30).

5.3.2 Case 2: Center Crack in Tension. Geometry of the center-cracked block having height (h = 40 mm), width (b = 40 mm), thickness (t = 40 mm) and through thickness crack length in the center (a = 6 mm) is shown in Fig. 10. The value of uniaxial tensile stress (σ) applied is 200 MPa. Von Mises and maximum principal for 3D center-cracked geometry is shown in Fig. 11 and 12, respectively. The difference between stress distributions for both form of alloy occurs due to their difference in elasto-plastic material properties. Size of the plastic zone ahead of the crack tip is much bigger in case of UFG form of the alloy as compared to its bulk form, which indicates its improved fracture resistance.

Figure 13 shows the strain energy release for the 3D center-cracked block of bulk and UFG 7075 Al alloy. Under same loading, geometric, and boundary conditions applied for both bulk and UFG alloy, strain energy release and external work are found higher in case of UFG alloy. Figure 14 shows stress values along the crack path. In this case, crack arrest took place in UFG alloy due to its high fracture energy and high stress requirement for local yielding.

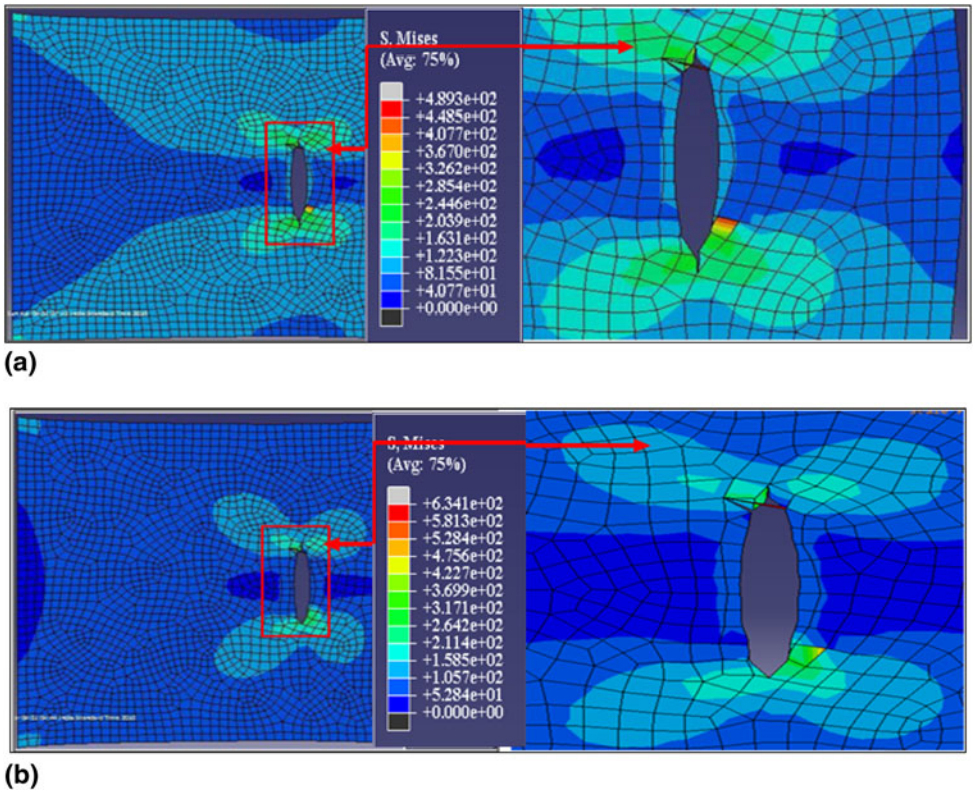

Fig. 24 A comparison of Von Mises stress distribution around crack tip. (a) Bulk 7075 Al alloy (zoomed view at the crack tip), (b) UFG 7075 Al alloy (zoomed view at the crack tip)

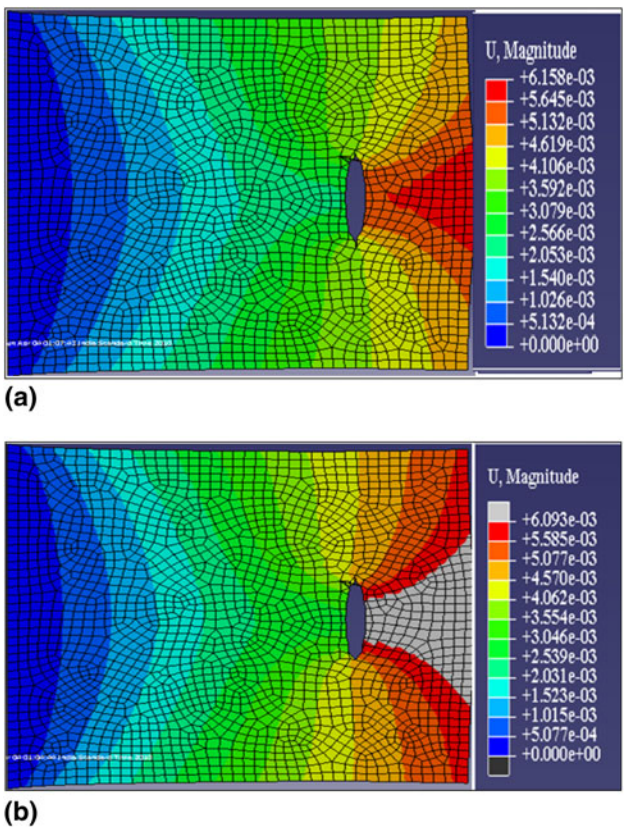

Fig. 25 A comparison of displacement field along with temperature distribution in the cracked plate. (a) Bulk 7075 Al alloy, (b) UFG 7075 Al alloy

5.3.3 Case 3: Three-Point Bend Specimen. To analyze the improved fracture behavior of UFG alloy, crack growth simulation are performed for a three-point bend (TPB) specimen, modeled according to ASTM standard E1820-09e1 (Ref 32). Figure 15 shows the schematic diagram of the crack growth behavior in TPB specimen. The geometry with 10 mm thickness and initial crack length (a) of 3 mm is loaded by quasi-static load of 3 kN.

Figure 16 represents the stress-strain state ahead of the crack tip. Von Mises stress distribution is shown for both form of alloy and the stress distribution is significantly higher in case of material. Crack growth is observed in case of bulk alloy whereas it gets arrested in the UFG form of alloy. The higher amount of plastic strain work ahead of the crack tip and bigger plastic zone size signifies the higher resistance towards crack propagation in UFG alloy as compared to its bulk form.

Figure 17 shows the comparative plots of strain energy release and external work for the TPB specimen of both bulk and UFG form of alloy. In this case also, the improved results are obtained in case of UFG alloy. The stress along crack path is plotted in Fig. 18.

5.3.4 Case 4: Compact Tension Specimen. Figure 19 shows the schematic diagram of the compact tension (CT) specimen modeled as per ASTM standard E1820-09e1 (Ref 33) to show the improved fracture behavior of the UFG 7075 alloy as compared to its bulk form. Crack growth behavior is analyzed in CT specimen for both form of the alloy under same geometric and loading conditions. The geometry with 10 mm specimen thickness, and initial crack length of 5 mm is loaded with 5 kN load. The results are found in good agreement with the earlier case studies presented in this work.

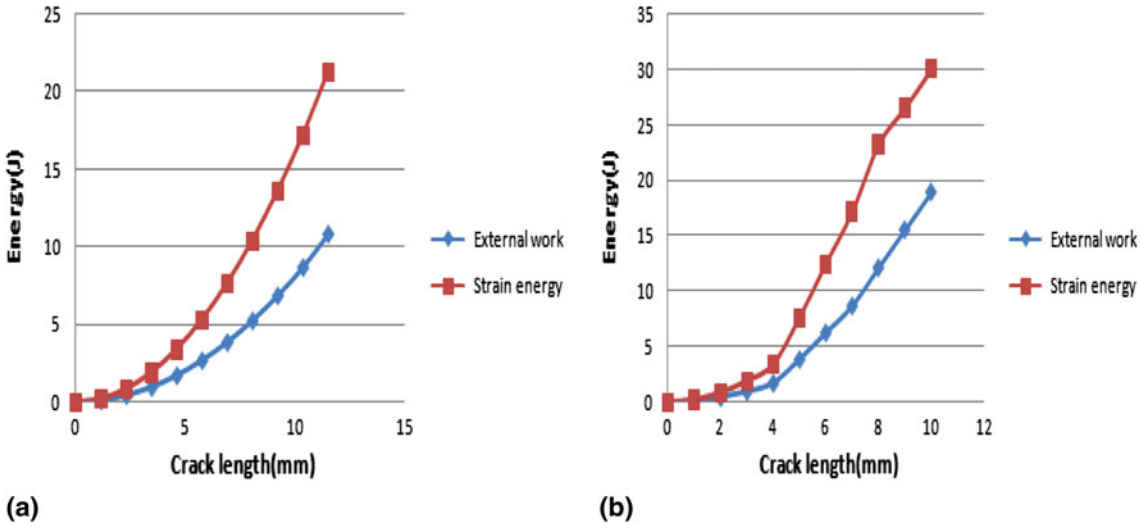

Fig. 26 A comparative plot of strain energy release for (a) bulk and (b) UFG 7075 Al alloy

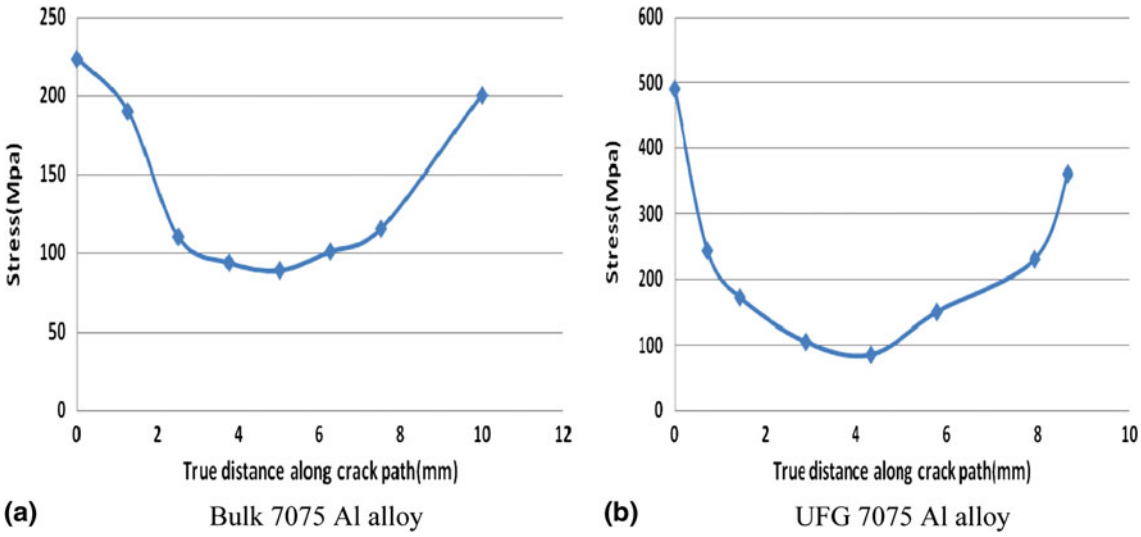

Fig. 27 A comparison of stress for (a) bulk and (b) UFG 7075 Al alloy

Figure 20 represents Von Mises stress distribution ahead of the crack tip for the CT specimen. Higher fracture energy explains the reason why crack does not advance in case of UFG alloy.

Figure 21 shows the strain energy release and external work for the CT specimen of both bulk and UFG form of the alloy. The stress values obtained along crack path are shown in Fig. 22. Higher strain energy release and stress values ahead of the crack tip explains better crack arrest capabilities of the UFG 7075 Al alloy.

5.3.5 Case 5: Temperature-Assisted Crack Growth in a Plate. The geometry of the cracked plate along with temperature distribution having height (H = 40 mm), width (B = 40 mm), thickness (t = 10 mm) and through thickness crack length parallel to the right edge (a = 10 mm) is shown in Fig. 23. The value of applied uniform pressure (P) is 100 MPa and coefficient of thermal expansion is 25.2×10^{-6} m/m°C. The geometry has been modeled by unstructured mesh using bilinear quadrilateral plain strain elements having (40×40) elements along the edges.

In this example along with mechanical loading (uniform pressure), temperature distribution is also applied in the cracked plate. Due to the temperature field applied, plastic deformation becomes easier for both the bulk and UFG form alloy and simultaneously a significant decrease in strain energy release for the fully cracked object can be seen as compared to other case studies. Plastic deformation is less in case of UFG alloy due to increase in hardening exponent due to cryorolling. Crack is arrested in the UFG form due to the reasons explained in earlier case studies. Figure 24 shows Von Mises stress distribution and Fig. 25 shows the displacement field along with temperature distribution in the cracked plate. In case of UFG alloy, global displacement is less in comparison to bulk alloy due to increase in hardening exponent after cryorolling.

Figure 26 shows the comparative plots of strain energy release and external work for the cracked plate under thermo-mechanical loading of both bulk and UFG form of the alloy. The stress along crack path is plotted in Fig. 27. The results are found in good agreement with earlier case studies.

6. Conclusions

The present study reports experimental evaluation of tensile, and impact toughness behaviour of bulk 7075 Al alloy and its ultrafine-grained form. A significant improvement in tensile and impact properties has been observed due to the grain fragmentation, high dislocation density, and stoppage of dynamic recovery achieved by rolling at liquid nitrogen atmosphere (cryorolling). The microstructure before and after the cryorolling characterized by FESEM, show an evidence of grain refinement. Grain refinement with the increasing cryorolling strain is also evident from the fracture surface morphology (characterized by FESEM) of the ultrafine-grained samples fractured under tensile and impact loading. XFEM simulations of crack growth were carried out using impact energy as the crack growth criterion. XFEM simulations revealed the effect of improved fracture energy over the crack growth properties of the alloy in its UFG form as compared to its bulk form. The impact energy obtained by Charpy testing used as the crack growth criterion under quasi-static loading conditions based on the Griffith energy concept. Elastic-plastic material properties such as YS, hardening exponent has been evaluated by tensile testing to carry out XFEM simulations of elastic-plastic ductile fracture ahead of the crack tip using the finite element software package ABAQUS.

Five case studies composed of real-life 3D problems and standard specimens are used to determine the fracture toughness and to demonstrate the use of new energy based crack growth simulation. The method is based on the fundamental Griffith energy concept thus having the potential of dealing with fracture problems that involve complex loading, material nonlinearity, large deformation, and path-dependent deformation processes. The results obtained from the case studies show that XFEM is an efficient and versatile method, and can be implemented in case of complex fracture problems.

The computation of the strain energy release, stress distribution ahead of the crack tip and study of crack propagation, and crack tip plastic zone simulations presented here to demonstrate the improved fracture behavior of UFG 7075 Al alloy as compared to the bulk alloy. The numerical examples also show that the crack growth took place in case of bulk 7075 Al alloy whereas it got arrested in case of UFG form of Al alloy under same loading, boundary, and geometric conditions. Moreover, the size of the plastic zone ahead of the crack tip is much bigger in case of UFG alloy as compared to bulk form which shows a significant improvement in the fracture toughness due to ultrafine-grain formation in cryorolling process.

Acknowledgment

One of the authors, Dr. R. Jayaganthan, expresses his sincere thanks to DST, New Delhi for the financial support to this work through Grant no. DST-462-MMD.

References

1. Y. Wang, M. Chen, F. Zhou, and E. Ma, High Tensile Ductility in a Nanostructured Metal, *Nature*, 2002, **419**, p 912–915
2. T.R. Lee, C.P. Chang, and P.W. Kao, The Tensile Behavior and Deformation Microstructure of Cryo-Rolled and Annealed Pure Nickel, *Mater. Sci. Eng. A*, 2005, **408**, p 131–135
3. S.K. Panigrahi and R. Jayaganthan, A Comparative Study on Mechanical Properties of Al 7075 Alloy Processed by Rolling at Cryogenic Temperature and Room Temperature, *Mater. Sci. Forum*, 2008, **584–586**, p 734–740
4. R. Jayaganthan and S.K. Panigrahi, Effect of Cryorolling Strain on Precipitation Kinetics of Al 7075 Alloy, *Mater. Sci. Forum*, 2008, **584–586**, p 911–916
5. Y.B. Lee, D.H. Shin, K.T. Park, and W.J. Nam, Effect of Annealing Temperature on Microstructures and Mechanical Properties of a 5083 Al Alloy Deformed at Cryogenic Temperature, *Scripta Mater.*, 2004, **51**, p 355–359
6. T. Shanmugasundaram, B.S. Murty, and V.S. Sarma, Development of Ultrafine Grained High Strength Al-Cu Alloy by Cryorolling, *Scripta Mater.*, 2006, **54**, p 2013–2017
7. X.M. Li and M.J. Stranik, Effect of Compositional Variations on Characteristics of Coarse Intermetallic Particles in Overaged 7000 Aluminium Alloys, *Mater. Sci. Technol.*, 2001, **17**, p 1324–1328
8. N. Sukumar and J.H. Prevost, Modeling Quasi-Static Crack Growth with the Extended Finite Element Method Part I. Computer Implementation, *Int. J. Solids Struct.*, 2003, **40**, p 7513–7537
9. R. Huang, N. Sukumar, and J.H. Prevost, Modeling Quasi-static Crack Growth with the Extended Finite Element Method Part II, Numerical Applications, *Int. J. Solids Struct.*, 2003, **40**, p 7539–7552
10. M.J. McNary, Implementation of the Extended Finite Element Method (XFEM) in the ABAQUS Software Package, Master Thesis, Georgia Institute of Technology, May 2009.
11. Z. Yang, An Energy-Based Crack Growth Criterion for Modelling Elastic-Plastic Ductile Fracture, *Mech. Res. Commun.*, 2005, **32**, p 514–524
12. C. Fan, P.Y. Ben Jar, and J.J. Roger Cheng, Prediction of Energy Release Rates for Crack Growth Using FEM-Based Energy Derivative Technique, *Eng. Fract. Mech.*, 2007, **74**, p 1243–1254
13. W. Li and T. Siegmund, An Analysis of Crack Growth in Thin-Sheet Metal Via a Cohesive Zone Model, *Eng. Fract. Mech.*, 2002, **69**, p 2073–2093
14. E. Giner, N. Sukumar, J.E. Tarancon, and F.J. Fuenmayor, An Abaqus Implementation of the Extended Finite Element Method, *Eng. Fract. Mech.*, 2009, **76**(3), p 347–368
15. J.H. Chen, Q. Wang, G.Z. Wang, and Z. Li, Fracture Behavior at Crack Tip—A New Framework for Cleavage Mechanism of Steel, *Acta Mater.*, 2003, **51**, p 1841–1855
16. D. Markovic and A. Ibrahimbegovic, Complementary Energy Based FE Modelling of Coupled Elasto-Plastic and Damage Behavior for Continuum Microstructure Computations, *Comput. Methods Appl. Mech. Eng.*, 2006, **195**, p 5077–5093
17. I.L. Lim, I.W. Johnston, and S.K. Choi, A Finite Element Code for Fracture Propagation Analysis Within Elasto-Plastic Continuum, *Eng. Fract. Mech.*, 1996, **53**(2), p 193–211
18. Z. Wang and T. Nakamura, Simulations of Crack Propagation in Elastic-Plastic Graded Materials, *Mech. Mater.*, 2004, **36**, p 601–622
19. N. Moes and T. Belytschko, Extended Finite Element Method for Cohesive Crack Growth, *Eng. Fract. Mech.*, 2002, **69**, p 813–833
20. A. Yazid, N. Abdelkader, and H. Abdelmadjid, A State-of-the-Art Review of the X-FEM for Computational Fracture Mechanics, *Appl. Math. Modell.*, 2009, **33**, p 4269–4282
21. T. Belytschko and T. Black, Elastic Crack Growth in Finite Elements with Minimal Remeshing, *Int. J. Numer. Methods Eng.*, 1999, **45**, p 601–620
22. M. Tajally, Z. Huda, and H.H. Masjuki, A Comparative Analysis of Tensile and Impact-Toughness Behavior of Cold-Worked and Annealed 7075 Aluminum Alloy, *Int. J. Impact Eng.*, 2010, **37**, p 425–432
23. J.G. Michopoulos, Directional Instability of Crack Propagation with Energy Dissipation, *Theor. Appl. Fract. Mech.*, 1988, **10**, p 177–189
24. S. Xu and X. Zhang, Determination of Fracture Parameters for Crack Propagation in Concrete Using an Energy Approach, *Eng. Fract. Mech.*, 2008, **75**, p 4292–4308
25. U. Tzadka and K. Schulgasser, Energy Approach to Crack Growth in a Fiber-Reinforced Brittle Material Modeled by an Inclusion, *Theor. Appl. Fract. Mech.*, 2009, **52**, p 72–82

26. ASTM Standard E8/E8M, 2009, "Standard Test Methods for Tension Testing of Metallic Materials," ASTM International, West Conshohocken PA, 2009. doi:10.1520/E0008-E0008M-09, www.astm.org
27. ASTM Standard E23, 2007ae1, "Standard Test Methods for Notched Bar Impact Testing of Metallic Materials," ASTM International, West Conshohocken PA, 2009. doi:10.1520/E0023-07AE01, www.astm.org
28. S.K. Panigrahi, R. Jayaganthan, and V. Pancholi, Effect of Plastic Deformation Conditions on Microstructural Characteristics and Mechanical Properties of Al 6063 Alloy, *Mater. Des.*, 2009, **30**, p 1894–1901
29. P. Das, R. Jayaganthan, and I.V. Singh, Tensile and Impact-Toughness Behaviour of Cryorolled Al 7075 Alloy, *Mater. Des.*, 2011, **32**(3), p 1298–1305
30. P. Das, R. Jayaganthan, T. Chowdhury, and I.V. Singh, Improvement of Fracture Toughness (K_{1c}) of 7075 Al Alloy by Cryorolling Process, *Mater. Sci. Forum*, 2011, **683**, p 81–94
31. P. Das, R. Jayaganthan, T. Chowdhury, and I.V. Singh, Fatigue Behaviour and Crack Growth Rate of Cryorolled Al 7075 Alloy, *Mater. Sci. Eng. A*, 2011, **528**, p 7124–7132
32. ABAQUS Analysis User's Manual (Version 6.9), United States of America, ABAQUS Inc., 2009
33. ASTM Standard E1820-09e1, "Standard Test Method for Measurement of Fracture Toughness," ASTM International, West Conshohocken PA, 2009. doi:10.1520/E1820-09E01, www.astm.org